Biochemistry

 Volume 42, Number 11 March 25, 2003

Current Topics

Insights into the Amyloid Folding Problem from Solid-State NMR

Robert Tycko*

Laboratory of Chemical Physics, National Institute of Diabetes and Digestive and Kidney Diseases, National Institutes of Health, Bethesda, Maryland 20892-0520

Received December 18, 2002; Revised Manuscript Received January 31, 2003

Amyloid fibrils are filamentous aggregates, with typical diameters of 10 nm and lengths on the order of microns, formed by a large class of peptides and proteins with disparate sequences and with molecular masses ranging from less than 1 kDa to tens of kilodaltons. Figure 1 shows typical amyloid fibrils as they appear in electron microscopy (EM)[1] measurements. Current interest in amyloid fibrils in the biomedical community stems from the fact that amyloid fibrils deposit in the affected organs of the so-called amyloid diseases (*1*). Several amyloid diseases, including Alzheimer's disease, type 2 diabetes, transmissible spongiform encephalopathies, and Parkinson's disease, constitute major public health problems. The precise role of amyloid deposits in these diseases has not been settled, but amyloid deposition is likely to be at least a contributing factor to their etiology (*2*, *3*). In the biophysical and biochemical communities, interest in amyloid fibrils additionally stems from the observation that the amyloid fibril appears to be a stable structural state of a generic polypeptide chain (*4*, *5*) and from the lack of a comprehensive explanation for this observation. At the level of EM images, amyloid fibrils formed by peptides and proteins with unrelated sequences appear at least similar, if not identical. Thus, amyloid fibrillization poses a problem that is opposite to the familiar protein folding problem. Whereas in the protein folding problem one seeks to understand how the diverse three-dimensional structures of proteins are determined uniquely by their amino acid sequences, in the amyloid folding problem one seeks to understand how a single structure can be common to a great many unrelated sequences.

Although amyloid fibrils formed by two different proteins may exhibit the same *morphology* in EM images, this is no guarantee that they share a common *molecular structure*. The most important barrier to solution of the amyloid folding problem has been the paucity of detailed structural information at the molecular level. Because amyloid fibrils are inherently noncrystalline and insoluble, determination of their molecular structures by the two principal experimental approaches to structure determination, i.e., X-ray crystallography and liquid-state nuclear magnetic resonance (NMR), has not been possible.

X-ray diffraction patterns of aligned amyloid fibrils exhibit a pronounced meridional scattering peak that corresponds to a characteristic spacing of 0.47−0.48 nm, assigned to the distance between peptide chains in β-sheets with a "cross-β" orientation (*6*, *7*), i.e., with the chain directions nearly perpendicular to the long axis of the fibril and the interchain hydrogen-bonding direction nearly parallel to the long axis. These β-sheets may span the entire length of the fibril. Nearly all other aspects of the molecular structures of amyloid fibrils have been unclear. Basic questions that have been unresolved include the following:

(1) What is the supramolecular organization of the cross-β motif? Are the β-sheets parallel or antiparallel? Does this depend on sequence?

* To whom correspondence should be addressed. Phone: 301-402-8272. Fax: 301-496-0825. E-mail: tycko@helix.nih.gov.

[1] Abbreviations: EM, electron microscope; NMR, nuclear magnetic resonance; Aβ_{n-m}, residues *n* through *m* of the Alzheimer's β-amyloid peptide; STEM, scanning transmission electron microscope; EPR, electron paramagnetic resonance; SANS, small-angle neutron scattering; MAS, magic-angle spinning; R^2, rotational resonance; fpRFDR-CT, constant-time finite-pulse radio frequency-driven recoupling; MQ, multiple quantum; 2D, two dimensional; CSA, chemical shift anisotropy; DQCSA, double-quantum chemical shift anisotropy; MPL, mass per length.

10.1021/bi027378p This article not subject to U.S. Copyright. Published 2003 by the American Chemical Society
Published on Web 02/26/2003

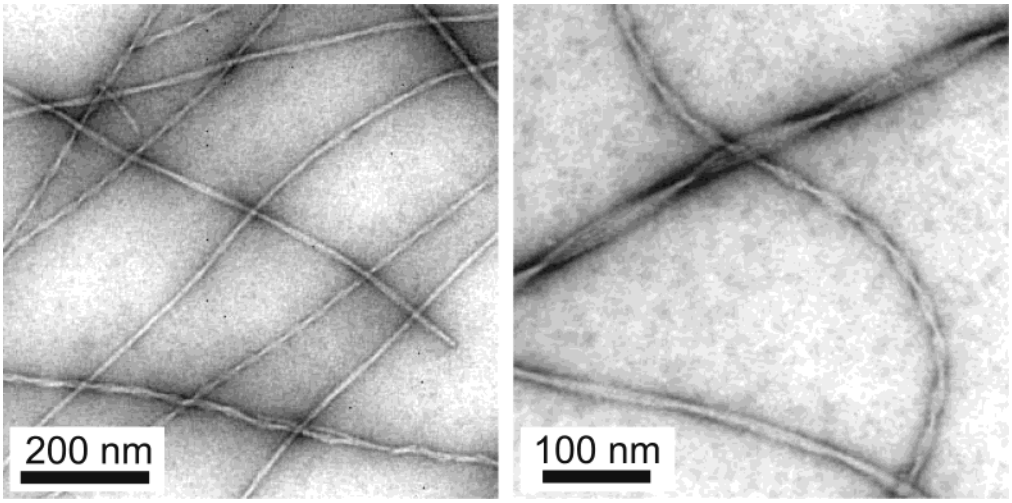

FIGURE 1: Transmission electron microscope images of amyloid fibrils formed by the 40-residue β-amyloid peptide associated with Alzheimer's disease (Aβ_{1-40}, sequence DAEFRHDSGY EVHHQKLVFF AEDVGSNKGA IIGLMVGGVV) from a 210 μM peptide solution in 10 mM phosphate buffer, pH 7.4, at 24 °C. Samples are negatively stained with uranyl acetate (*8*). The thinnest Aβ_{1-40} fibrils, called protofilaments, have 5 ± 1 nm diameters. Thicker fibrils appear to be twisted pairs or bundles of protofilaments.

(2) Which segments of the amino acid sequence form the β-strands? Do other segments adopt non-β-strand secondary structures?

(3) What is the degree of structural order at the molecular level in amyloid fibrils?

(4) Which intramolecular and intermolecular interactions stabilize amyloid fibril structures, in addition to the interchain backbone hydrogen bonding in the β-sheets?

(5) Which aspects of amyloid fibril structures are universal? Which are sequence-specific?

(6) In the case of amyloid fibrils formed by proteins with well-ordered monomeric or oligomeric structures, which structural elements of the monomeric or oligomeric form are retained in the amyloid fibril form?

Since 1999, our laboratory has been using solid-state NMR methods to examine the molecular structures of amyloid fibrils, primarily fibrils formed by the full-length, 40-residue β-amyloid peptide associated with Alzheimer's disease (Aβ_{1-40}) (*8*−*10*), by the 42-residue variant of this peptide (Aβ_{1-42}) (*11*), and by fragments of Aβ_{1-40} that serve as model systems (*11*, *12*). Our solid-state NMR data address the questions listed above and lead to a structural model for Aβ_{1-40} fibrils. The remainder of this paper describes the basic principles behind the solid-state NMR measurements, the types of information available from these measurements, and our specific findings for amyloid fibrils. Important contributions to the structural characterization of amyloid fibrils by solid-state NMR have also been made by Griffin and co-workers (*13*, *14*) and by Lynn, Meredith, Botto, and co-workers (*15*−*18*).

Several other physical techniques have recently been brought to bear on amyloid fibril structure determination, including cryo-EM (*19*−*21*), scanning transmission electron microscopy (STEM) (*11*, *22*), atomic force microscopy (*23*−*25*), electron paramagnetic resonance (EPR) (*26*, *27*), and small-angle neutron scattering (SANS) (*18*, *28*). To a large extent, these techniques provide structural constraints that are complementary to constraints from solid-state NMR in terms of length scale and site specificity. Studies of amyloidogenic peptides and proteins by liquid-state NMR provide important information about precursors to fibrillization (*29*−*32*), as well as indirect information about likely fibril structures (*33*, *34*).

Sources of Structural Information in Solid-State NMR

The term "solid-state NMR" simply means nuclear magnetic resonance spectroscopy of solids and other condensed phases of matter that are not isotropic liquids. Differences between solid-state and liquid-state NMR techniques and data ultimately arise from the absence of the rapid isotropic tumbling and translational diffusion of molecules in liquids, which accounts for the very high resolution and relative simplicity of liquid-state NMR spectra. One important technological difference is that many solid-state NMR measurements are carried out under magic-angle spinning (MAS), i.e., rapid sample rotation about an axis at the "magic angle" $\theta_m = \cos^{-1}(1/\sqrt{3})$, to achieve spectral resolution and sensitivity approaching that of liquid-state NMR. One important difference in the data is that scalar couplings and nuclear Overhauser effects, which are often the dominant sources of structural information in liquid-state NMR, are relatively unimportant in solid-state NMR. Several types of solid-state NMR measurements and features of solid-state NMR data have proven useful in the structural characterization of amyloid fibrils, as follows.

Measurements of the direct magnetic interactions between pairs of nuclear spins, called dipole−dipole couplings, serve as measurements of interatomic distances (see Figure 2). In a rigid solid, the strength of the dipole−dipole coupling between nuclei I and S is represented by the coupling constant $d = \gamma_I\gamma_S\hbar/(2\pi R^3)$, where γ_I and γ_S are the nuclear gyromagnetic ratios, $\hbar$ is Planck's constant, and R is the distance. For a pair of ^{13}C nuclei, $d = 69$ Hz at $R = 0.48$ nm (the characteristic spacing between β-strands in a parallel or antiparallel β-sheet). For a ^{13}C−^{15}N pair, $d = 28$ Hz at $R = 0.48$ nm. Although these couplings are weak, they can be measured reliably with appropriate radio frequency pulse sequence techniques, to better than 10% precision in R under realistic experimental conditions. Techniques for measuring dipole−dipole couplings under MAS conditions are commonly called "dipolar recoupling" methods, because these

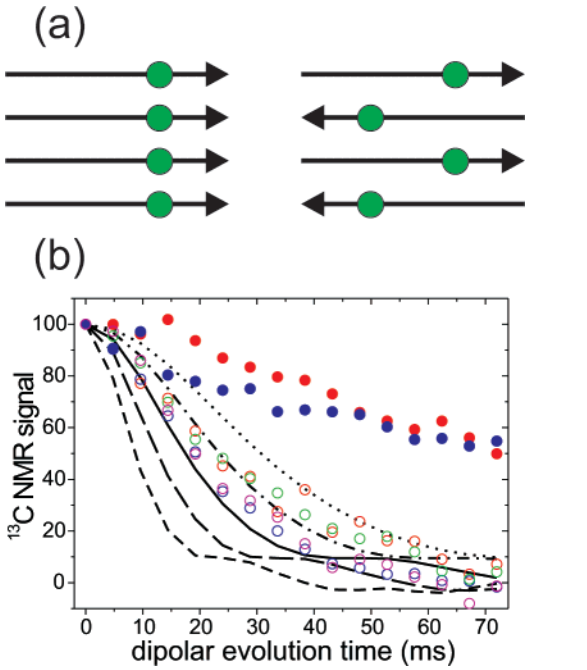

FIGURE 2: Determination of the supramolecular organization of β-sheets in Aβ_{1-40} fibrils by measurements of ^{13}C−^{13}C nuclear magnetic dipole−dipole couplings with the fpRFDR-CT technique (*9*, *38*). (a) Synthesis of Aβ_{1-40} peptides with a single ^{13}C label (green circles) leads to a chain of ^{13}C nuclei with spacings of approximately 0.48 nm in an in-register, parallel β-sheet and to significantly larger internuclear distances in an antiparallel β-sheet. (b) Experimental fpRFDR-CT decays for Aβ_{1-40} fibrils with ^{13}C labels at backbone carbonyl sites of V12 (blue circles), F20 (green circles), L34 (magenta circles), and V39 (red circles). Filled circles are data for unfibrillized samples, showing that the intermolecular ^{13}C−^{13}C distances decrease significantly upon fibril formation. Corrections for natural-abundance ^{13}C NMR signal contributions are applied as described (*9*). Simulated decays are shown for distances of 0.38 nm (short dashes), 0.43 nm (long dashes), 0.48 nm (solid line), 0.53 nm (dot−dashed line), and 0.58 nm (dotted line). These data indicate an in-register, parallel alignment of hydrogen-bonded peptide chains in Aβ_{1-40} fibrils.

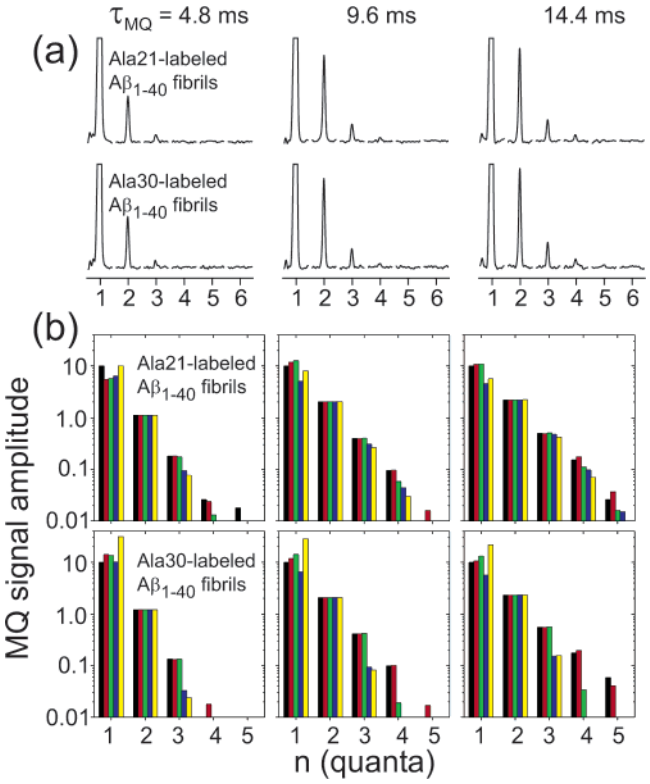

FIGURE 3: Determination of the supramolecular organization of β-sheets in Aβ_{1-40} fibrils by solid-state MQ ^{13}C NMR (*8*, *41*). (a) Experimental MQ excitation spectra for samples labeled at methyl carbons of A21 or A30, i.e., in the two hydrophobic segments of Aβ_{1-40}. Significant three-quantum and four-quantum signals develop with increasing MQ excitation time τ_{MQ}, with nearly identical amplitudes for the two samples. (b) Comparison of experimental MQ signal amplitudes (black bars) with simulations (*8*) for a fully parallel β-sheet structure (red bars), a fully antiparallel structure (yellow bars), and mixed structures in which parallel trimers (green bars) or parallel dimers (blue bars) pack in an antiparallel fashion. Fully parallel simulations agree best with the experimental data.

techniques restore couplings that would otherwise be averaged to zero by MAS. Dipolar recoupling methods that have been applied to amyloid fibrils include rotational resonance (*35*) (R^2), dipolar recoupling with a windowless sequence (*36*), rotational echo double resonance (*37*) (REDOR), and constant-time finite-pulse radio frequency-driven recoupling (*38*) (fpRFDR-CT). These methods have been used both to measure intermolecular distances between specific isotopically labeled sites in β-strands, and thereby determine the supramolecular organization of the cross-β motifs (*9*, *11*, *13*, *15*−*18*), and to measure intramolecular distances that place constraints on secondary structure at specific sites (*10*, *16*, *17*, *39*). Distances are determined from dipolar recoupling data by comparison of the experimental signal decay or build-up curves with numerical simulations, as in Figure 2.

Dipole−dipole couplings also permit the excitation and detection of multiple quantum (MQ) NMR signals in ^{13}C-labeled amyloid fibrils. In MQ NMR measurements, one detects nuclear spin transitions in which groups of spins flip simultaneously in the magnetic field of the NMR spectrometer (*40*, *41*). An *n*-quantum ^{13}C NMR signal is observable only if at least *n* ^{13}C nuclei are sufficiently close in space to be linked by a network of couplings with coupling constants $d \sim 1/\tau_{MQ}$, where τ_{MQ} is the period for excitation of MQ coherences in the pulse sequence. As shown in Figure 3, we have used MQ ^{13}C NMR to differentiate between parallel and antiparallel β-sheets and, in the case of parallel β-sheets in Aβ_{1-40} fibrils, to establish that the parallel alignment of peptide chains extends over at least four successive chains (i.e., to rule out alternations between parallel and antiparallel alignments) (*8*, *11*, *12*, *42*).

Dipolar recoupling and MQ NMR measurements have been performed primarily, although not exclusively (*10*, *42*, *43*), on amyloid fibril samples with ^{13}C and/or ^{15}N labeling of one or two sites per peptide molecule. The relatively sharp solid-state NMR lines observed for singly and doubly labeled Aβ fibrils under MAS encouraged us to prepare samples with uniform ^{13}C- and ^{15}N-labeling of multiple residues and to apply two-dimensional (2D) MAS NMR techniques to these samples (*10*, *12*, *44*, *45*) (see Figure 4). The 2D spectra contain at least two essential pieces of structural information: (1) isotropic ^{13}C chemical shifts of CO, C_α, and C_β sites correlate strongly with secondary structure (*46*−*50*), allowing identification of the residues that participate in β-strands and residue-specific identification of non-β-strand conformations; (2) ^{13}C and ^{15}N MAS NMR line widths are empirical indicators of structural order, allowing identification of ordered and disordered segments of the amino acid sequence within amyloid fibrils. By combining uniform

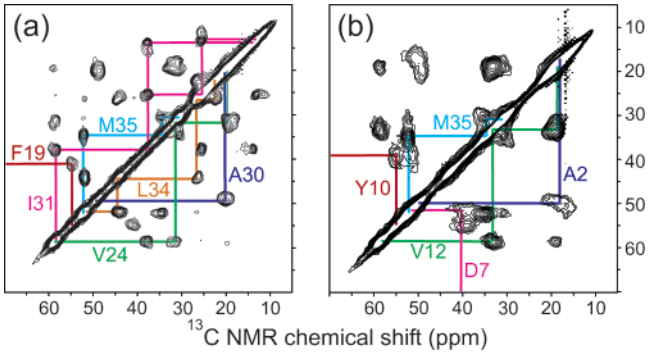

FIGURE 4: 2D $^{13}C-^{13}C$ NMR exchange spectra of Aβ_{1-40} fibrils with uniform ^{13}C-labeling of selected residues. Spectra are obtained in a 9.4 T magnetic field with high-speed MAS (*10*, *12*, *44*). Only the aliphatic regions of the spectra are shown. Strong cross-peaks connect chemical shifts of directly bonded ^{13}C-labeled sites. Chemical shifts of individual sites, which indicate the local secondary structure, are determined from the color-coded assignment paths. (a) Sample labeled at F19, V24, G25, A30, I31, L34, and M35. (b) Sample labeled at A2, D7, G9, Y10, V12, and M35. Significantly broader cross-peaks for A2, D7, and Y10 indicate structural disorder of the N-terminal segment of Aβ_{1-40} in the fibrils.

labeling of multiple residues with 2D spectroscopy, one can map the secondary structure and structural order across the entire peptide sequence with a relatively small number of fibril samples (*10*, *12*, *44*).

Quantitative constraints on the backbone and side chain torsion angles that define the peptide conformation at specific residues are available from several sources. As depicted in Figure 5, measurement of the distance between two sequential backbone carbonyl carbons in a doubly ^{13}C-labeled peptide constrains the backbone ϕ angle between the two ^{13}C labels (*10*, *16*, *17*, *39*). Techniques that directly probe the relative orientation of two bond vectors or of two functional groups and thereby provide direct angular information have also been developed and are called "tensor correlation" methods. In the case of a doubly carbonyl-labeled peptide, constraints on both backbone torsion angles ϕ and ψ of a single residue can be obtained with techniques that probe the relative orientations of the ^{13}C chemical shift anisotropy (CSA) tensors at the two labeled sites, including 2D MAS exchange spectroscopy (*51*) and double-quantum CSA (DQCSA) spectroscopy (*52*). Data obtained with these techniques are analyzed by comparison with numerical simulations, as in Figure 5. Tensor correlation methods that are applicable to samples with multiple uniformly labeled residues have also been described (*53*−*55*). Measurements of backbone torsion angles by tensor correlation methods can serve as a confirmation and refinement of ϕ and ψ values predicted from chemical shift data for regular secondary structural elements (*10*, *44*) and as a means of determining backbone conformations in segments where the chemical shift data do not provide reliable ϕ and ψ predictions (*10*, *39*).

The success of solid-state NMR studies of amyloid fibrils to date provides new impetus for methodological developments. Promising new sources of information include $^{13}C_\alpha$ CSA tensor measurements (*56*), proton-mediated $^{13}C-^{13}C$ exchange spectroscopy (*57*), frequency-selective dipolar recoupling methods (*43*), and solid-state ^1H NMR under ultra-high-speed MAS (*58*).

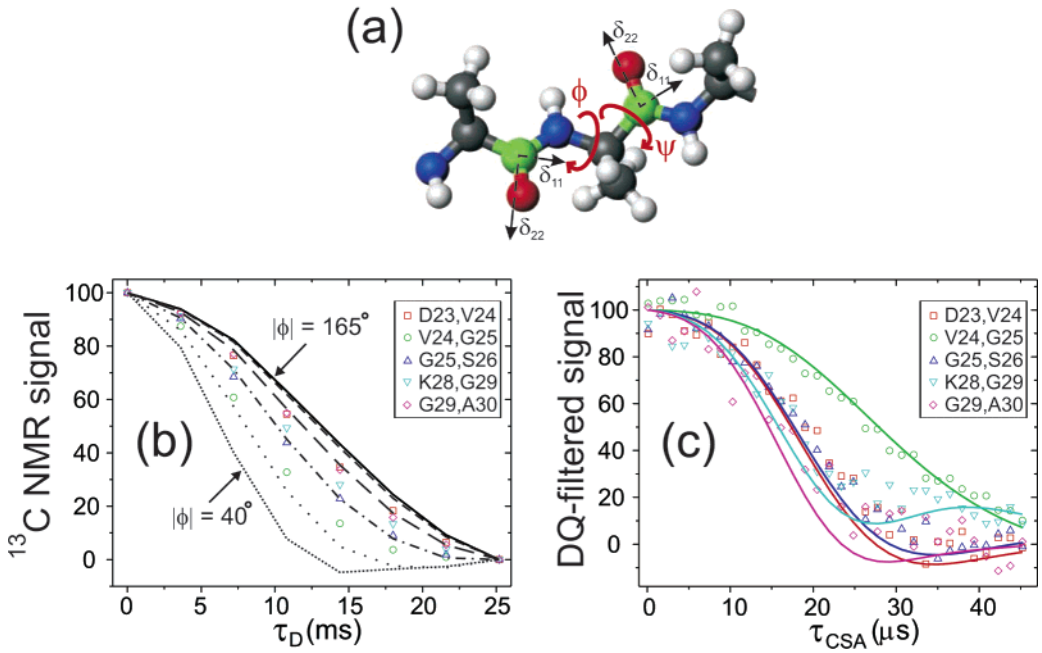

FIGURE 5: Determination of peptide backbone torsion angles ϕ and ψ from solid-state NMR measurements on doubly ^{13}C-labeled peptides. (a) Segment of a peptide backbone with ^{13}C labels (green atoms) at two sequential carbonyl sites. Measurements of the dipole−dipole coupling strength, which depends on the $^{13}C-^{13}C$ distance, constrain ϕ. Measurements of the relative orientation of the two carbonyl groups, through the relative orientation of the CSA tensor axes (δ_{11} and δ_{22}), constrain both ϕ and ψ. (b) Experimental fpRFDR-CT data for Aβ_{1-40} fibril samples with carbonyl ^{13}C labels at the indicated sites and simulations for $|\phi|$ values from 40° to 165° in 25° increments. Data and simulations are baseline-corrected to minimize contributions from background signals. τ_D is the effective dipolar evolution period in the fpRFDR-CT technique (*38*). (c) DQCSA data for the same samples. τ_{CSA} is the CSA evolution period for DQ coherences in this technique (*52*). Lines are simulations for $\phi,\psi = -145°,115°$ (red), $-70°,-40°$ (green), $68°,-65°$ (blue), $-120°,-125°$ (cyan), and $-165°,-133°$ (magenta). These torsion angle values represent best fits to the combined data on doubly labeled Aβ_{1-40} samples (*10*, *39*).

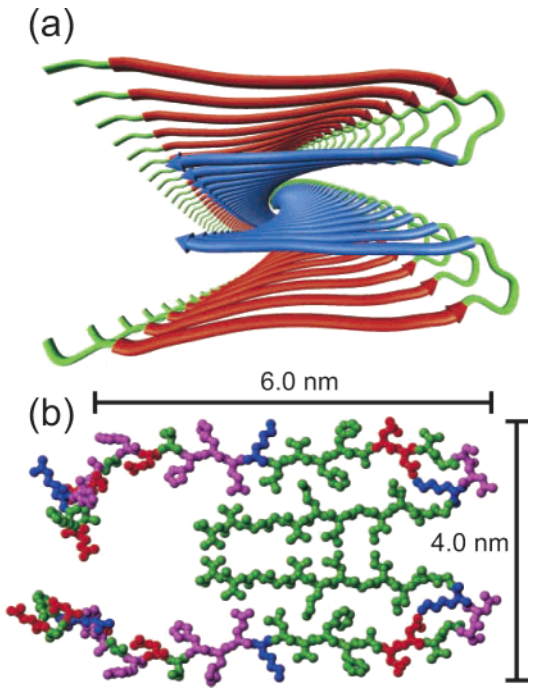

FIGURE 6: Structural model for Aβ_{1-40} protofilaments, derived by energy minimization with constraints based on solid-state NMR data (*10*). The model is also consistent with overall dimensions and MPL from EM and STEM and with the characteristic spacings in X-ray fiber diffraction patterns. (a) Ribbon representation of residues 9−40, viewed down the long axis of the protofilament. Each molecule contains two β-strands (red and blue) that form separate parallel β-sheets in a double-layered cross-β motif. Two such cross-β units comprise the protofilament, which is then a four-layered structure. (b) Atomic representation of residues 1−40 with color coding to indicate residues with hydrophobic (green), polar (magenta), positively charged (blue), and negatively charged (red) side chains. Backbone C═O and N−H bond vectors are approximately perpendicular to the page. Contacts between β-sheet layers are through side chain−side chain interactions. N-Terminal residues are assigned random conformations to indicated structural disorder. Contacts between the two cross-β units are assumed to be along the hydrophobic faces created by side chains of the C-terminal segment. The core of the protofilament is hydrophobic with the exception of the oppositely charged side chains of D23 and K28, which form salt bridges.

Results for Full-Length β-Amyloid Fibrils

Our ongoing studies of Aβ_{1-40} fibrils have generated sufficient structural constraints to permit the development of a structural model (see Figure 6) by constrained energy minimization (*10*). Although not all aspects of this model are uniquely determined by experimental data, the model is consistent with a large body of data that includes measurements of intermolecular distances by fpRFDR-CT (*9*), MQ ^{13}C NMR spectra (*8*), ^{13}C and ^{15}N chemical shift and line width measurements from 2D spectroscopy (*10*), torsion angle constraints from tensor correlation measurements (*10*, *39*), fibril dimensions observed in EM images (*8*, *10*), X-ray diffraction data (*59*), and measurements of the mass per length (MPL) of Aβ fibrils by STEM (*11*, *22*). The condition that the β-strands in amyloid fibrils form a cross-β motif is a particularly important constraint, as it requires the β-strands to be positioned with all of their backbone C═O and N−H bonds nearly parallel to a single axis (i.e., the long axis of the fibril). Once the β-strand segments are identified from ^{13}C chemical shifts and the alignment and registry of β-strands within a β-sheet are determined from dipolar recoupling and MQ NMR data, relatively few degrees of freedom remain. These degrees of freedom are further restricted by the fibril dimensions and MPL data. In short, significantly fewer structural constraints per residue are required to determine the correct "fold" of an amyloid fibril than are typically required for monomeric globular proteins. Features of the model in Figure 6 that are supported by the experimental data are as follows:

(i) Approximately the first 10 residues of Aβ_{1-40} are structurally disordered in the fibrils, as indicated by relatively large ^{13}C MAS NMR line widths (*10*) (>3 ppm for CO, C$_\alpha$, and C$_\beta$ sites in residues 2−9 versus <2.5 ppm in residues 12−39) and by significantly weaker intermolecular ^{13}C−^{13}C dipole−dipole couplings than in the remainder of the sequence (*8*, *9*). The N-terminal segment is susceptible to proteolysis both in vivo (*60*) and in vitro (*61*) and is not required for fibril formation (*62*, *63*).

(ii) Residues 12−24 and 30−40 form two β-strand segments that are separated by a "bend" segment with non-β-strand conformations at G25, S26, and G29. These secondary structure elements are indicated by ^{13}C chemical shifts in 2D spectra and by tensor correlation data (*10*, *39*).

(iii) The two β-strand segments form two separate parallel β-sheets. In-register, parallel alignment of the peptide chains from G9 to V39 is indicated by intermolecular ^{13}C−^{13}C dipole−dipole couplings detected in dipolar recoupling and MQ NMR measurements on a series of singly ^{13}C-labeled samples (*8*, *9*). The net bend angle of 180° in residues 24−29 in Figure 6, which brings the two β-sheets in contact through side chain−side chain interactions, is consistent with the dimensions of the narrowest Aβ_{1-40} fibrils observed in EM images, called "protofilaments", which have widths of 5 ± 1 nm. Without a large net bend between the two β-strands, the structurally ordered part of each Aβ_{1-40} molecule would have a length of approximately 10 nm, at variance with the observed protofilament widths. Thus, a single molecular layer in the cross-β motif, which we refer to as a single "cross-β unit", is a double-layered β-sheet in this model.

(iv) Protofilaments with minimum width and MPL are constructed from two cross-β units. The MPL of a single cross-β unit would be 9.0 kDa/nm, equal to the 4.33 kDa molecular mass of Aβ_{1-40} divided by the 0.48 nm intermolecular spacing. Histograms of MPL values extracted from STEM images of Aβ_{1-40} fibrils (*22*) show a peak near 18 kDa/nm but no counts near 9.0 kDa/nm. In Figure 6, the two cross-β units make contact at the hydrophobic surfaces created by side chains of residues 30−40. This mode of association seems plausible on physical grounds and results in a four-layered model with cross-sectional dimensions that closely match the minimum fibril widths observed experimentally and with distances between β-sheet layers that agree well with the 8.9 nm spacing suggested by equatorial scattering peaks in fiber diffraction data (*59*). Fibrils with larger widths, which typically exhibit morphologies suggesting that they are twisted pairs or bundles of finer filaments (see Figure 1), may be formed by lateral association of these protofilaments. Contacts between protofilaments in a paired or bundled fibril may be along β-sheet surfaces, through a combination of hydrophobic interactions (possibly involving V18 and F20) and electrostatic interactions (possibly involving K16 and E22) (*10*).

The model in Figure 6 resolves an important fundamental issue regarding the intermolecular interactions that stabilize Aβ_{1-40} fibrils. It has been argued that fibrillization of full-length Aβ and fragments thereof is driven by hydrophobic interactions (*63*−*66*). The experimental observation that the β-sheets in Aβ_{1-40} fibrils have an in-register, parallel structure can be attributed to the fact that such a structure maximizes contacts among hydrophobic side chains. However, an in-register, parallel β-sheet structure also places all charged side chains in rows with spacings on the order of 0.5 nm. In the low dielectric environment that may exist in the interior of an amyloid fibril, repulsions between like charges could destabilize the fibril structure by roughly 70 kcal/mol, overwhelming the stabilizing effect of the hydrophobic contacts (estimated to be of order 2 kcal/mol). In Figure 6b, the only charged side chains in the interior are D23 and K28, which form salt bridges that may actually stabilize the structure. Apart from D23 and K28, the protofilament structure has a purely hydrophobic core. Other charged and polar side chains are on the exterior of the structure, in a high dielectric environment as the fibrils grow in aqueous solution. ^{13}C and ^{15}N chemical shifts indicate that side chains of D23 and K28 are indeed charged in Aβ_{1-40} fibrils grown at pH 7.4. Dipole−dipole couplings between the side chain carboxylate carbon of D23 and the side chain amino nitrogen of K28 indicate an interatomic distance of roughly 0.4 nm, consistent with salt bridge formation (*10*).

Aβ_{1-40} and other amyloid fibrils exhibit a diversity of morphologies in EM images (*20*, *67*), as in Figure 1. It has been argued that morphological differences simply reflect differences in the lateral association of protofilaments (*20*), suggesting that the molecular structure within the protofilament would be essentially identical in all morphologies. In our laboratory, evidence is accumulating that fibrils with different morphologies may actually contain protofilament structures that are different at the molecular level. In the case of Aβ_{1-40} fibrils, the most significant variations in molecular structure appear to be in the conformation of the bend region (residues 25−29). Although we have observed sample-to-sample variations in chemical shifts for residues 12−21 and 30−35, the CO, C_α, and C_β chemical shifts are always indicative of β-strand conformations. More significant chemical shift variations are observed for residues 23, 24, 25, 28, and 29. Fibrillization protocols that permit preparation of fibrils with predominantly a single molecular structure, as indicated by a single set of backbone ^{13}C chemical shifts, are under development.

Although the 40-residue form of full-length Aβ is present at highest concentrations in the human body, it has been shown that elevated levels of the 42-residue form (Aβ_{1-42}, with additional hydrophobic I31 and A42 residues at the C-terminus) are associated with familial forms of Alzheimer's disease (*68*) and that Aβ_{1-42} peptides are the major component of immature senile plaques and cerebrovascular amyloid deposits (*69*, *70*). In vitro, Aβ_{1-42} forms fibrils more rapidly and at lower concentrations than Aβ_{1-40} (*71*, *72*). Solid-state NMR measurements indicate the same in-register, parallel alignment of peptide chains in β-sheets in Aβ_{1-42} fibrils as demonstrated for Aβ_{1-40} fibrils (*11*). Recent EPR measurements support in-register, parallel β-sheets, as well as other aspects of the model described above, in both Aβ_{1-40} and Aβ_{1-42} fibrils prepared with pairs of nitroxide spin labels (*26*). EM images show that Aβ_{1-42} fibrils have similar morphologies and nearly the same dimensions as Aβ_{1-40} fibrils. STEM measurements indicate that the Aβ_{1-42} protofilament contains two cross-β units, as discussed above for the Aβ_{1-40} protofilament (*11*). These data suggest that the association of Aβ_{1-42} with familial Alzheimer's disease is due to lower equilibrium solubility or more rapid fibrillization kinetics, rather than being a consequence of structural differences.

Results for β-Amyloid Fragment Fibrils

Many shorter peptides derived from the full-length Aβ sequence (denoted Aβ_{n-m} for residues *n* through *m*) also form amyloid fibrils. Structural studies of these fibrils provide further insight into the generality of the model in Figure 6 and the interactions that stabilize amyloid fibril structures.

Aβ_{10-35} has proven to be a useful model system for full-length Aβ (*32*, *73*) because, apart from a shorter C-terminal hydrophobic segment, it contains the structurally ordered portion of the full-length peptide. Extensive dipolar recoupling measurements on singly ^{13}C-labeled Aβ_{10-35} fibrils by Lynn, Meredith, Botto, and co-workers (*15*−*18*) provided the first experimental demonstration of in-register, parallel β-sheets in amyloid fibrils when previous work had suggested or assumed that the cross-β motifs in amyloid fibrils were constructed from antiparallel β-sheets (*63*, *74*−*79*). Recent MQ NMR, fpRFDR-CT, and REDOR measurements on Aβ_{10-35} fibrils also indicate in-register, parallel β-sheets (*11*). STEM measurements show that Aβ_{10-35} protofilaments contain two cross-β units (*11*), as discussed above for Aβ_{1-40} and Aβ_{1-42} fibrils. Thus, the molecular structure of Aβ_{10-35} fibrils may resemble that of full-length Aβ fibrils. A detailed structural model for the cross-β unit in Aβ_{10-35} fibrils that is quite similar to the model in Figure 6 has been developed independently by Ma and Nussinov, on the basis of the solid-state NMR data of Lynn, Meredith, Botto, and co-workers, computer modeling, and molecular dynamics simulations (*80*).

A model for Aβ_{10-35} fibrils that differs qualitatively from that in Figure 6, especially in terms of the peptide conformation and the degree of β-sheet lamination, has been proposed by Lynn and co-workers (*15*, *17*, *18*). In this model, the peptide has a fully extended conformation, the protofilament has approximately six β-sheet layers, as supported by MPL values determined from SANS data (*18*) and by cross-linking data (*15*), and protofilaments interact laterally along their edges (*18*), rather than along β-sheet surfaces. Strain that might exist in this model if residues 10−35 formed a single β-sheet is relieved by dynamic fluctuations in intermolecular hydrogen bonding (*81*). The apparent disagreement between measurements of MPL for Aβ_{10-35} fibrils by SANS and by STEM may arise from differences in pH, with greater lateral association of protofilaments or lamination of β-sheets occurring at higher pH (*11*, *82*), or from basic differences in the properties of the two measurements, with STEM measurements focusing on selected filaments on an EM grid and SANS measurements sampling all fibrils in an aqueous environment.

Fibrils formed by certain other Aβ fragments have qualitatively different molecular structures. Aβ_{16-22} (sequence KLVFFAE, with acetyl and amide capping groups at the N-

and C-termini, respectively) forms amyloid fibrils in which the β-sheets have an antiparallel structure, with hydrogen bonds between residues $16 + k$ and $22 - k$, where k is an integer between 0 and 6 (*12*). This experimental observation can be rationalized by noting that either a parallel or an antiparallel alignment of Aβ_{16-22} chains could maximize hydrophobic contacts, while an antiparallel structure permits intermolecular pairing of oppositely charged K16 and E22 side chains.

Amyloid fibrils formed by Aβ_{34-42} have been shown by Lansbury, Griffin, and co-workers to have an antiparallel β-sheet structure, for which a detailed structural model was developed primarily from measurements of intramolecular and intermolecular dipole−dipole couplings with the R^2 technique (*13*). These studies were the first application of solid-state NMR to the problem of amyloid fibril structure. As in the case of Aβ_{16-22}, either a parallel or an antiparallel β-sheet structure could maximize hydrophobic contacts in Aβ_{34-42} fibrils. The antiparallel β-sheet structure may be preferred because of the more favorable electrostatic interactions between C-terminal carboxylate and N-terminal amino groups.

As a final example, fibrils formed by Aβ_{11-25} (sequence EVHHQKLVFFAEDVG, no capping of N- and C-termini) have been the subject of structural studies by X-ray fiber diffraction (*6*, *83*), cryo-EM (*21*), and infrared spectroscopy (*84*). On the basis of diffraction data (*83*), Serpell et al. have proposed a unit cell and space group for the Aβ_{11-25} fibril structure, as well as a molecular structure in which Aβ_{11-25} molecules form β-hairpins with a type I β-turn in residues 17−20 and intramolecular hydrogen bonding between antiparallel β-strands formed by residues 11−16 and 21−25. ^{13}C chemical shift and dipolar recoupling data for Aβ_{11-25} fibrils prepared in our laboratory at pH 2.5 and 7.4 are inconsistent with the β-hairpin structural model (unpublished data). These solid-state NMR data indicate that residues 17−21 form β-strands in antiparallel β-sheets with purely intermolecular hydrogen bonding. Interestingly, the registry of hydrogen bonds revealed by the dipolar recoupling data is different at the two pH values, reflecting the pH dependence of side chain ionization states and the influence of electrostatics on β-sheet organization.

What Do the Results Say about Amyloid Folding?

The experimental findings discussed above provide at least partial answers to the questions raised in the introductory section:

(1) While antiparallel β-sheets are found in amyloid fibrils formed by certain Aβ fragments, the cross-β motif in full-length Aβ fibrils is comprised of in-register, parallel β-sheets. Thus, the supramolecular structure in amyloid fibrils is not determined uniquely by the amino acid sequence at the level of 15-residue or shorter segments. In all cases, the β-sheet structures appear to maximize hydrophobic contacts. Short peptides with a single hydrophobic segment may then adopt either parallel or antiparallel structures, while peptides with an asymmetric distribution of hydrophobic segments adopt parallel structures. The β-sheet structures in amyloidogenic peptides without hydrophobic segments have not yet been examined by solid-state NMR.

(2) The β-strand segments in amyloid fibrils can be identified by solid-state NMR, most easily through measurements of ^{13}C chemical shifts. In the case of Aβ_{1-40} fibrils, the structurally ordered β-strand segments are less than 15 residues in length and are separated by a non-β-strand bend segment that may be capable of adopting distinct conformations in distinct fibril morphologies.

(3) Line widths observed in 2D NMR spectra of amyloid fibrils indicate a high degree of structural order, approaching that observed in protein crystals. Structurally disordered segments that presumably lie outside the fibril core, such as the N-terminal segment of Aβ_{1-40}, are also observed. Although a structural biologist accustomed to studying the highly ordered molecular structures of monomeric proteins and protein complexes might assume that amyloid fibrils are ordered at the molecular level, this assumption would be an unproven hypothesis in the absence of the solid-state NMR data. It is not yet clear why amyloid fibril structures are not more highly disordered, given the lack of stringent sequence requirements for amyloid fibril formation, the predominantly one-dimensional nature of intermolecular interactions in amyloid fibrils, and the likelihood that the energetic cost of defects involving shifts in the registry of intermolecular hydrogen bonds would be low.

(4) All full-length Aβ and Aβ fragment fibrils studied to date have been found to possess structures that maximize hydrophobic contacts within a β-sheet. Thus, hydrophobic interactions appear to play a large role in stabilizing amyloid fibril structures. A dominant role for hydrophobic interactions has been suggested by other experimental results as well (*63*−*66*). However, electrostatic repulsions within the core of the fibril must also be avoided. The model in Figure 6 indicates how electrostatic destabilization of an in-register, parallel β-sheet structure can be prevented by an appropriate molecular conformation in an amyloid fibril.

(5) Although the cross-β structural motif is a universal and defining property of amyloid fibrils, the supramolecular organization of the β-sheets within this motif has been shown to depend on the amino acid sequence. Thus, no truly universal amyloid fibril structure exists. Nonetheless, there may be classes of peptides and proteins that share similar molecular structures in their amyloid state.

(6) Since the Aβ peptides are flexible (*29*, *31*) or have nonregular secondary structures (*32*) as monomers in aqueous solution, the issue of which structural features in the monomeric or oligomeric state are retained in the fibrillar state is irrelevant in this case. Prelimary solid-state NMR data on amyloid fibrils formed by insulin indicate that the helical segments in the native tetrameric form are not retained in fibril form (unpublished data, with M. A. Weiss). On the other hand, studies of the enzymatic activity of amyloid fibrils formed by enzyme/amyloidogenic peptide fusion proteins demonstrate convincingly that the globular structures of the enzyme components are preserved in the fibrils (*85*).

Future Prospects

Determination of the full molecular structures of amyloid fibrils, primarily through a combination of solid-state NMR and EM measurements, now appears experimentally feasible. Further refinement and validation of the model for Aβ_{1-40} fibrils in Figure 6 will depend on additional measurements of backbone and side chain torsion angles and on identification of intramolecular and intermolecular side chain−side

chain contacts. Solid-state NMR techniques capable of providing this information in an efficient manner are under active development (*43*, *53*−*55*). In addition, techniques that are specifically applicable to aligned samples, such as those employed in structural studies of silks (*86*), may provide new types of structural constraints.

As research along these lines progresses, it is likely that new insights into the mechanism of action of fibrillization inhibitors (*87*−*90*), the molecular structures of fibrillization intermediates (*91*), and the mechanisms of fibril growth (*92*, *93*) will be forthcoming. Additional experiments will clarify the extent to which amyloid fibril structures resemble those of β-helical proteins, as suggested by several groups (*79*, *94*, *95*), and the possible role of domain swapping in amyloid fibrillization (*96*). The inferred importance of side chain hydrogen bonding in glutamine- and asparagine-rich amyloidogenic peptides (*97*) and of particular electrostatic interactions (*98*) will be tested by direct structural measurements. We are entering an era in which our molecular level understanding of amyloid fibrils will approach that of globular proteins.

ACKNOWLEDGMENT

EM images in Figure 1 were obtained by Drs. A. T. Petkova and R. D. Leapman. Solid-state NMR data in Figures 2−5 were obtained by Drs. J. J. Balbach, N. A. Oyler, O. N. Antzutkin, and A. T. Petkova. Dr. Y. Ishii developed methodology applied in Figures 2, 4, and 5. Dr. F. J. Blanco developed methodology applied in Figure 5. I additionally acknowledge contributions to this work by Drs. G. Buntkowsky, M. A. Weiss, F. Dyda, D. J. Gordon, and S. C. Meredith.

REFERENCES

1. Sipe, J. D. (1992) *Annu. Rev. Biochem. 61*, 947−975.
2. Eikelenboom, P., et al. (2002) *Glia 40*, 232−239.
3. Hoppener, J. W. M., Ahren, B., and Lips, C. J. M. (2000) *N. Engl. J. Med. 343*, 411−419.
4. Chiti, F., et al. (1999) *Proc. Natl. Acad. Sci. U.S.A. 96*, 3590−3594.
5. Fandrich, M., and Dobson, C. M. (2002) *EMBO J. 21*, 5682−5690.
6. Inouye, H., Fraser, P. E., and Kirschner, D. A. (1993) *Biophys. J. 64*, 502−519.
7. Sunde, M., et al. (1997) *J. Mol. Biol. 273*, 729−739.
8. Antzutkin, O. N., et al. (2000) *Proc. Natl. Acad. Sci. U.S.A. 97*, 13045−13050.
9. Balbach, J. J., et al. (2002) *Biophys. J. 83*, 1205−1216.
10. Petkova, A. T., et al. (2002) *Proc. Natl. Acad. Sci. U.S.A. 99*, 16742−16747.
11. Antzutkin, O. N., Leapman, R. D., Balbach, J. J., and Tycko, R. (2002) *Biochemistry 41*, 15436−15450.
12. Balbach, J. J., et al. (2000) *Biochemistry 39*, 13748−13759.
13. Lansbury, P. T., et al. (1995) *Nat. Struct. Biol. 2*, 990−998.
14. Griffiths, J. M., et al. (1995) *J. Am. Chem. Soc. 117*, 3539−3546.
15. Benzinger, T. L. S., et al. (1998) *Proc. Natl. Acad. Sci. U.S.A. 95*, 13407−13412.
16. Gregory, D. M., et al. (1998) *Solid State Nucl. Magn. Reson. 13*, 149−166.
17. Benzinger, T. L. S., et al. (2000) *Biochemistry 39*, 3491−3499.
18. Burkoth, T. S., et al. (2000) *J. Am. Chem. Soc. 122*, 7883−7889.
19. Jimenez, J. L., et al. (1999) *EMBO J. 18*, 815−821.
20. Jimenez, J. L., et al. (2002) *Proc. Natl. Acad. Sci. U.S.A. 99*, 9196−9201.
21. Serpell, L. C., and Smith, J. M. (2000) *J. Mol. Biol. 299*, 225−231.
22. Goldsbury, C. S., et al. (2000) *J. Struct. Biol. 130*, 217−231.
23. Stine, W. B., et al. (1996) *J. Protein Chem. 15*, 193−203.
24. Harper, J. D., Lieber, C. M., and Lansbury, P. T. (1997) *Chem. Biol. 4*, 951−959.
25. Goldsbury, C., Kistler, J., Aebi, U., Arvinte, T., and Cooper, G. J. S. (1999) *J. Mol. Biol. 285*, 33−39.
26. Torok, M., et al. (2002) *J. Biol. Chem. 277*, 40810−40815.
27. Serag, A. A., Altenbach, C., Gingery, M., Hubbell, W. L., and Yeates, T. O. (2002) *Nat. Struct. Biol. 9*, 734−739.
28. Yong, W., et al. (2002) *Proc. Natl. Acad. Sci. U.S.A. 99*, 150−154.
29. Barrow, C. J., and Zagorski, M. G. (1991) *Science 253*, 179−182.
30. Sticht, H., et al. (1995) *Eur. J. Biochem. 233*, 293−298.
31. Riek, R., Guntert, P., Dobeli, H., Wipf, B., and Wuthrich, K. (2001) *Eur. J. Biochem. 268*, 5930−5936.
32. Zhang, S., et al. (2000) *J. Struct. Biol. 130*, 130−141.
33. Liu, K., Kelly, J. W., and Wemmer, D. E. (2002) *J. Mol. Biol. 320*, 821−832.
34. Viles, J. H., et al. (2001) *Biochemistry 40*, 2743−2753.
35. Raleigh, D. P., Levitt, M. H., and Griffin, R. G. (1988) *Chem. Phys. Lett. 146*, 71−76.
36. Gregory, D. M., et al. (1995) *Chem. Phys. Lett. 246*, 654−663.
37. Gullion, T., and Schaefer, J. (1989) *J. Magn. Reson. 81*, 196−200.
38. Ishii, Y., Balbach, J. J., and Tycko, R. (2001) *Chem. Phys. 266*, 231−236.
39. Antzutkin, O. N., Balbach, J. J., and Tycko, R. (2003) *Biophys. J.* (submitted for publication).
40. Weitekamp, D. P. (1983) in *Advances in Magnetic Resonance* (Waugh, J. S., Ed.) pp 111−274, Academic Press, New York.
41. Antzutkin, O. N., and Tycko, R. (1999) *J. Chem. Phys. 110*, 2749−2752.
42. Oyler, N. A., and Tycko, R. (2002) *J. Phys. Chem. B 106*, 8382−8389.
43. Jaroniec, C. P., Tounge, B. A., Herzfeld, J., and Griffin, R. G. (2001) *J. Am. Chem. Soc. 123*, 3507−3519.
44. Ishii, Y. (2001) *J. Chem. Phys. 114*, 8473−8483.
45. Baldus, M., Petkova, A. T., Herzfeld, J., and Griffin, R. G. (1998) *Mol. Phys. 95*, 1197−1207.
46. Saito, H. (1986) *Magn. Reson. Chem. 24*, 835−852.
47. Wishart, D. S., Sykes, B. D., and Richards, F. M. (1991) *J. Mol. Biol. 222*, 311−333.
48. Iwadate, M., Asakura, T., and Williamson, M. P. (1999) *J. Biomol. NMR 13*, 199−211.
49. Cornilescu, G., Delaglio, F., and Bax, A. (1999) *J. Biomol. NMR 13*, 289−302.
50. Laws, D. D., et al. (2001) *Proc. Natl. Acad. Sci. U.S.A. 98*, 11686−11690.
51. Weliky, D. P., and Tycko, R. (1996) *J. Am. Chem. Soc. 118*, 8487−8488.
52. Blanco, F. J., and Tycko, R. (2001) *J. Magn. Reson. 149*, 131−138.
53. Feng, X., et al. (1997) *J. Am. Chem. Soc. 119*, 12006−12007.
54. Rienstra, C. M., et al. (2002) *J. Am. Chem. Soc. 124*, 11908−11922.
55. Hong, M. (1999) *J. Magn. Reson. 139*, 389−401.
56. Yao, X. L., and Hong, M. (2002) *J. Am. Chem. Soc. 124*, 2730−2738.
57. Lange, A., Luca, S., and Baldus, M. (2002) *J. Am. Chem. Soc. 124*, 9704−9705.
58. Ishii, Y., Yesinowski, J. P., and Tycko, R. (2001) *J. Am. Chem. Soc. 123*, 2921−2922.
59. Malinchik, S. B., Inouye, H., Szumowski, K. E., and Kirschner, D. A. (1998) *Biophys. J. 74*, 537−545.
60. Roher, A. E., et al. (1993) *J. Biol. Chem. 268*, 3072−3083.
61. Kheterpal, I., Williams, A., Murphy, C., Bledsoe, B., and Wetzel, R. (2001) *Biochemistry 40*, 11757−11767.
62. Pike, C. J., Overman, M. J., and Cotman, C. W. (1995) *J. Biol. Chem. 270*, 23895−23898.
63. Hilbich, C., Kisterswoike, B., Reed, J., Masters, C. L., and Beyreuther, K. (1991) *J. Mol. Biol. 218*, 149−163.
64. Hilbich, C., Kisterswoike, B., Reed, J., Masters, C. L., and Beyreuther, K. (1992) *J. Mol. Biol. 228*, 460−473.
65. Halverson, K., Fraser, P. E., Kirschner, D. A., and Lansbury, P. T. (1990) *Biochemistry 29*, 2639−2644.
66. Harper, J. D., Wong, S. S., Lieber, C. M., and Lansbury, P. T. (1999) *Biochemistry 38*, 8972−8980.
67. Goldsbury, C. S., et al. (1997) *J. Struct. Biol. 119*, 17−27.
68. Iwatsubo, T. (1999) *Acta Histochem. Cytochem. 32*, 13−15.
69. Iwatsubo, T., et al. (1994) *Neuron 13*, 45−53.

70. Roher, A. E., et al. (1993) *Proc. Natl. Acad. Sci. U.S.A. 90*, 10836−10840.
71. Harper, J. D., Wong, S. S., Lieber, C. M., and Lansbury, P. T. (1997) *Chem. Biol. 4*, 119−125.
72. Jarrett, J. T., Berger, E. P., and Lansbury, P. T. (1993) *Biochemistry 32*, 4693−4697.
73. Esler, W. P., et al. (1996) *Biochemistry 35*, 13914−13921.
74. Fraser, P. E., et al. (1992) *Biochemistry 31*, 10716−10723.
75. Tjernberg, L. O., et al. (1999) *J. Biol. Chem. 274*, 12619−12625.
76. Li, L. P., Darden, T. A., Bartolotti, L., Kominos, D., and Pedersen, L. G. (1999) *Biophys. J. 76*, 2871−2878.
77. Chaney, M. O., Webster, S. D., Kuo, Y. M., and Roher, A. E. (1998) *Protein Eng. 11*, 761−767.
78. George, A. R., and Howlett, D. R. (1999) *Biopolymers 50*, 733−741.
79. Lazo, N. D., and Downing, D. T. (1998) *Biochemistry 37*, 1731−1735.
80. Ma, B. Y., and Nussinov, R. (2002) *Proc. Natl. Acad. Sci. U.S.A. 99*, 14126−14131.
81. Lakdawala, A. S., Morgan, D. M., Liotta, D. C., Lynn, D. G., and Snyder, J. P. (2002) *J. Am. Chem. Soc. 124*, 15150−15151.
82. Thiyagarajan, P., et al. (2000) *J. Appl. Crystallogr. 33*, 535−539.
83. Serpell, L. C., Blake, C. C. F., and Fraser, P. E. (2000) *Biochemistry 39*, 13269−13275.
84. Fraser, P. E., et al. (1994) *J. Mol. Biol. 244*, 64−73.
85. Baxa, U., Speransky, V., Steven, A. C., and Wickner, R. B. (2002) *Proc. Natl. Acad. Sci. U.S.A. 99*, 5253−5260.
86. Asakura, T., Ito, T., Okudaira, M., and Kameda, T. (1999) *Macromolecules 32*, 4940−4946.
87. Tjernberg, L. O., et al. (1996) *J. Biol. Chem. 271*, 8545−8548.
88. Soto, C., Kindy, M. S., Baumann, M., and Frangione, B. (1996) *Biochem. Biophys. Res. Commun. 226*, 672−680.
89. Lowe, T. L., Strzelec, A., Kiessling, L. L., and Murphy, R. M. (2001) *Biochemistry 40*, 7882−7889.
90. Gordon, D. J., Sciarretta, K. L., and Meredith, S. C. (2001) *Biochemistry 40*, 8237−8245.
91. Kirkitadze, M. D., Condron, M. M., and Teplow, D. B. (2001) *J. Mol. Biol. 312*, 1103−1119.
92. Lomakin, A., Teplow, D. B., Kirschner, D. A., and Benedek, G. B. (1997) *Proc. Natl. Acad. Sci. U.S.A. 94*, 7942−7947.
93. Pallitto, M. M., and Murphy, R. M. (2001) *Biophys. J. 81*, 1805−1822.
94. Perutz, M. F., Finch, J. T., Berriman, J., and Lesk, A. (2002) *Proc. Natl. Acad. Sci. U.S.A. 99*, 5591−5595.
95. Wille, H., et al. (2002) *Proc. Natl. Acad. Sci. U.S.A. 99*, 3563−3568.
96. Liu, Y. S., Gotte, G., Libonati, M., and Eisenberg, D. (2001) *Nat. Struct. Biol. 8*, 211−214.
97. Perutz, M. F., Johnson, T., Suzuki, M., and Finch, J. T. (1994) *Proc. Natl. Acad. Sci. U.S.A. 91*, 5355−5358.
98. Tjernberg, L., Hosia, W., Bark, N., Thyberg, J., and Johansson, J. (2002) *J. Biol. Chem. 277*, 43243−43246.

BI027378P